A Curvelet-Based Morphological Segmentation of Abdominal CT Images

M. Sakalli[1], T. D. Pham[2], K. M. Lam[3], and H. Yan[4]

Abstract— **This paper presents a segmentation methodology of abdominal axial CT images. The aim of the study is to determine the location of mesenteric area from the axial images so the organs enclosed within can be localized precisely for diagnostic purposes. The challenge confronted here is that there is no a certain deterministic shape of abdominal organs. The methodology implemented here utilizes a curvelets stage followed by morphological image processing to achieve a contour emphasized segmentation from the gestalts of surrounding organs. This paper gives a detailed analysis of approach taken with the problems faced and a brief comparison wrt to other wavelet approaches.**

Index Terms— **curvelets, wavelets, abdominal image segmentation, non-maximal suppression, edge and contour detection, non-maximal suppression, connected-components labeling.**

I. INTRODUCTION

There is no a specific one simple algorithm to locate objects in cluttered environments. Problem gets even tougher with the objects having varying texture and contour characters. To achieve a successful localization requires a preprocessing stage of images to enhance the ROI which is a low-level image processing. This follows a segmentation stage and then involves further rendering of object classification to distinguish the organs of interest. Here, our focus is to detect mesentery from CT images and later on the bowels in particular. The mesentery is an evaginated reflection of the peritoneum connecting bowels to the posterior abdominal wall. As well intestines, some other organs included within abdominal viscera are like stomach, liver and biliaryduck system, pancreas, spleen, kidneys, ureters. The positions of the abdominal viscera vary with the activities, posture, respiration, degree of filling, and with the gravity. Therefore, radiological evaluations cannot have a fixed model, as studies have shown that "the normal abdominal viscera have no fixed shapes and no fixed positions, and every quantification must take into account the conditions existing at the time of observation. It is reported in [2], [1] such that profound variations of position may be caused not only by mechanical forces but also by mental influences. An efficient semi/fully automatic organ segmentation which can at least be suggestive to guide physicians, is essential to avoid uncertainties leading to correct diagnosis. It is hard to design such a system accurate enough within the error-tolerance of physicians reaching to the ground-truth with a minimum false-segmentation rate.

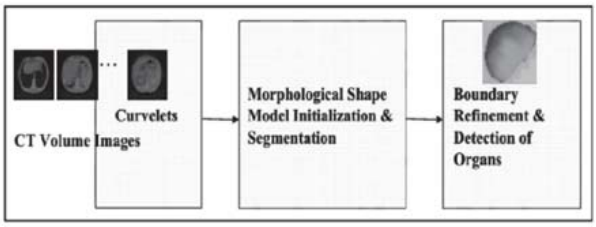

Fig. 1. Block diagram of our methodology in three stages, curvelet decomposition, morphological enhancement, segmentation, and assignment of organs to the boundaries, with respect to a trained dictionary of organs.

Our approach has three stages as presented in Fig. 1, the first stage is curvelets, here assumption is that organs have rather circular details. By employing curvelets we don't just eliminate redundant details but we aim to enhance the image for the related circular features, in Section II. The subsequent step is morphological stage where segmentation is performed to obtain gestalt features of organs in terms of contours. Idea here is to obtain an approximate translation and rotation free silhouette of organs with their surrounding organs III. The third stage in section IV focuses on evaluation of contours to eliminate those organs whose shapes and positions and their neighborhood criteria are easy to determine their anatomical properties. Maximal meaningful alignment by entropic exclusion (Helmholtz grouping principle) is applied here. We determine surrounding muscles and vertebrate, and then we engulf the possible area of interest. Such a methodology, excluding unambiguous symptoms and regions is a well-known common method applied in diagnostics to approximate anomalies [3]. In sections V, and VI we discuss existing techniques and the results of our algorithm.

II. CURVELETS

We employ curvelets to develop contours around at the vicinity of possible edge details with a rather thick stroke of brash. Curvelets are applied in various fields [6] not just for denoising of images but also to capture surface like singularities detecting future descriptors in multidimensional volumetric data involving medical imaging, seismic imaging, video processing and computer vision. Wavelets decompose images at every decomposition level into four subbands from the lowest to the higher frequency bands, in horizontal, vertical and diagonal directions. The lowest frequency band coefficients are nondirectional $\varphi^2(x, y) =$

*This work was funded by The University of Aizu, Fukushima, JP, 11/2012-03/2014.

*Publication is supported by Scientific Research Projects Committee of Marmara University, BAPKO. FEN-D-050614-0246.

[1]M. Sakalli is with Dept of CSE, Faculty of Eng, Marmara University. <msakalli at marmara.edu.tr>

[2]T. Pham is with The University of Aizu-Wakamatsu, Fukushima, JP

[3]K. M. Lam is with Dept of EIE, The Hong Kong Polytechnic Univ.

[4]H. Yan is with Computer Eng Dept of EE, City Univ. of Hong Kong.

$\varphi(x)\varphi(y)$ associated with mother wavelet function $|\phi|$, and filtering is applied in a separable manner. Similarly wavelet coefficients are $\psi(1)(x,y) = \varphi(x)\cdot\psi(y)$, $\psi(2)(x,y) = \varphi(y)\cdot\psi(x), \psi(3)(x,y) = \psi(x)\cdot\psi(y)$, for the three directions given above, respectively. While they are good in compact piecewise approximations in 1D, and sensitive to the sharp-point singularities (in 0D), they are not anisotropic, and blind to the smoothness of the first order features and unable to isolate lines or curvy features. These limitations are addressed by the ridgelet transforms by capturing 1D line singularities, but they are also inefficient to capture curvature-kind 2nd order features [9].

A comparative review of directional wavelets addressing geometric features in particular (Steerable wavelets, Gabor wavelets, wedgelets, beamlets, bandlets [7], contourlets, shearlets, wave atoms, platelets, and surfacelets) as group of X-lets wrt curvelets is presented in references [6], [13]. In reference [8], directional, multiscale edge detection is proposed through M×M channels decomposed image with orthogonal and linear-phase M-band wavelet filters, such that each decomposition could contribute to the results in zero-crossings at the edge locations in different directions and resolutions. In recent decades the behavior of neural cells are characterized by X-lets, selective in scale for example in mammalian primary cortex, and selective in orientation in visual cortex [14], [15]. Similarly contourlets are reported in reference [18] for detecting bowel tumors, where, it is also reported that contourlet offer less clear directional features with more oscillations.

Considering a scale function $\Phi_j(x)$ in scale $j = 0$ for curvelets such that its Fourier Transform $\hat{\phi}_j(w_1, w_2) = U_j\{w_1, w_2\}$, $U(.,.)$ is the window defined in polar coordinates. In [10], $\phi_j(x)$ is explicitly referred as "mother curvelet" from which all curvelets at scale 2^{-j} are obtained by the equispaced sequence of rotations of θ_l, and translations of k_i, where $k_i \in \{k_1, k_2\} \in \mathbf{Z}^2$, $\theta_l = 2\pi\cdot 2^{-j/2}\cdot l$ with $l = 0, 1, ...$ The support of $U_j(r,\theta)$ is *a polar wedge*. defined by the support of windows, radial window $W(r)$ taking smooth, non-negative and real valued arguments and an angular window $V(t)$ taking real arguments and both obeying admissibility conditions. Window widths and lengths change with the scale in each direction. Curvelet family is defined as $\phi_{j,l,k}(x) = \phi(R_{\theta_l}(x - x_j{}^{l,k}))$ where R_{θ_l} is the rotation by θ radians, at scale j, and position $x_j{}^{l,k}$ Similar to wavelet transforms, the full curvelet transform consists of coarse scale lowest frequency band are $\Phi_{j_0,k}$ which are non-directional coefficients, and the directional finescale curvelet bands, with the elements $\phi_{j>j_0,l,k}$. Our interest is on the behavior of the fine-scale directional elements, to determine the strength of the for the contour and boundaries at the currentwedge. Although curvelet transform is not orthogonal, its transformation is invertible in both continuous and discrete domains. The choice of scale 2^{-j}, $j \geq 0$, and the equadistance of rotation angles $\theta_{j,l} = \pi l 2^{\lceil j/2\rceil}/2$ with $l = 0, 1, ..., 4.2^{\lceil j/2\rceil} - 1$, and with rotation matrix R_θ having the positions $b^{j,l}_{k1,k2} = R^{-1}_{\theta_{j,l}}(k1/2^j, k2/2^{j/2})^T$ lead to a discrete curvelet transformation (DCT) and form a tight frame satisfying Parseval's relation. Therefore, the $f(x_1, x_2) \in \mathbf{L}^2$ of image can be expanded by taking its inner products with curvelets, in the form of $f = \sum\langle f, \phi_{j,l,k}\rangle\phi_{j,l,k}$. Two methodologies to obtain DC coefficients, are FDCT by utilizing unequally spaced FFT, and FDCT by wrapping as detailed in references [10], [11]. The difference is mainly on the choice of spatial grids employed to translate curvelets at each scale and angle. Curvelet coefficients are obtained by IFFT of partitioned coefficients that are obtained as a result of $\{wedgewrapping\{FFT(f) * FFT(spatialwedge(\varphi)\}\}$. To decompose images, we use curvelab toolbox in MATLAB, (www.curvelet.org). In Fig. 2, an axial CT image is decomposed into a number of subbands, figure presents the energy of the coefficients. Fig. 3, is to make their localized energy sum explicit.

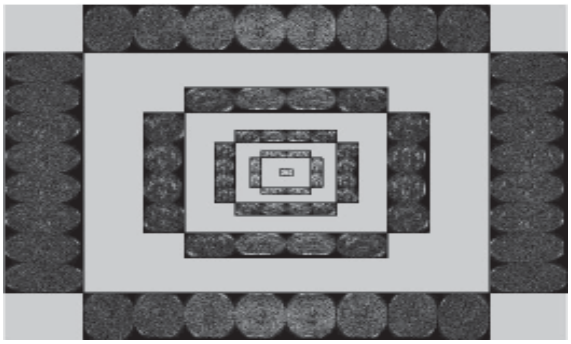

Fig. 2. For $l = 5$ scale curvelet decomposed abdominal image with the number of rotations $l = 8$. The number of curvelet bands at every scale is $l * 2.^{\lceil((j-[j:-1:2])/2\rceil} = [8, 16, 16, 32]$. Observe the tangential details around contour in each rotation. "www.ceremade.dauphine.fr/peyre/matlab/"

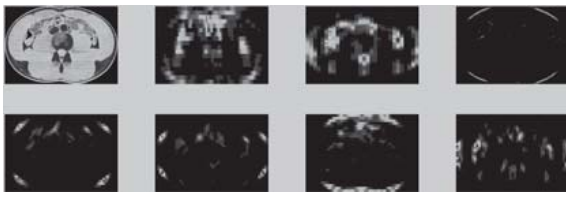

Fig. 3. Sum of the subbands as localized energy of DCT coefficients to give an emphasis on circular discontinuities.

III. Morphological Contour detection

A straightforward application is that the curvelet coefficients thresholded could offer an appearance of organs. But such an approach of thresholding require continuous and tedious manual intervention for repetitive forward and backward experimenting of soft and hard thresholds to determine the upper and lower intensity levels not even for a complete abdominal ROI under examination. Here our aim is rather to approximate a definite silhouette of organs and discard other isolated edges of small details. This suggests to utilize morphological filters. We take the approach similar to the scheme applied with Canny edge detection in [12] with curvelet coefficients, with an exception, we put emphasis on morphological filters instead of canny edge detectors. To underline, Canny edge detection in fact partially covers

Fig. 4. Inverse FDCTed image after non-maximal-suppression applied.

morphological filters in non-maximal suppression stage as presented below.

The correspondence from curvelet coefficients to the pixels requires special attention. Because at each decomposition level the resolution is determined by the DCT, although each curvelet coef has a specific fixed orientation l_i and located at a certain location k_1, k_2 of the subband (curveband) at level l. The decomposition depth is determined empirically. We consider the curvelet bands from 2nd to P-1, P is the last finest level and we map coarser level directional features, over finer levels gradually as presented in [12]. A directional orientation map is obtained in two steps, firstly we take the absolute sum effect of the magnitudes of the coefficients and then determine the dominant direction as the argmax of directions and record both the strength of the orientation and the direction as its dominant angle of the location. To eliminate undesired superfluous edges in parallel and contour deviations at the vicinity of strong edges, we employed non-maximal suppression to suppress those having weak gradient within the same curveband. (Fig. 4).

With curvelets, there is no need to check every angle with fine increments as it happens in usual non-maximal suppression check wrt every pixel offset in x and y with a specified radius. Instead we check angles $\pm 2\pi/(l_i)$, where l_i is the number of the curvebands at every level. All operations are performed in curvebands, 2 to $l_i/2$ since the other half of the curvebands are symmetric. The radius of non-maximal suppression is scaled between $3-1.2$ pixels from level $P-1$ to 2 because the distance between boundaries initially are assumed to be not less then $4-3$ pixels, which is something depends on the adjacency of the organs against each other and here we further perform morphological operations (consecutive opening and closing operations with different structuring elements set for ROI of organs) to eliminate adjacent pixels both marked as local maxima.

Finally we obtain contour boundaries emphasized by using Otsu's thresholding, and label the internal segments by using methodology of connected-components labeling. It wasn't always possible to achieve a precise segmentation due to the various factors mostly due to the inflexibility of the thresholding and complexity of the CT images. However, this segmentation provided a platform to alleviate the segmentation problem to the higher levels of matching against a template and apply possible amendments.

IV. Anatomical assignment of segmented regions: Boundary evaluation

In the previous sections CT images are treated as gray level images with no consideration of the anatomical topology. The outcome is not always perfect boundaries, in some cases the image of the organs seem to be over segmented or merged each other (Fig.5). At this stage we adopt a two-stage, regenerative, and discriminative model based registration of abdominal 2D axial intersections, with a sketchy silhouettes library of the visceral organs. In regenerative stage, a weighed match of organs in adjacent groups is taken account, and in the discriminative step, the organ based registration of silhouettes is adopted. Consider a closed contour signal $y \in R^n$ as linear combination of basic dictionary elements d_j, taken from an overcomplete dictionary $D \in R^{n,K}$ by an underdetermined equation $y = Dx$, such that where $x \in R^K$ and $j = 1...K$. In sparse form this equation has many solutions, it is possible to have a unique but non-sparse solution with many nonzero elements, in $min_x||x||_2$ sense, and the the solution, $x = D^T(DD^T)^{-1}y = D^+y.$, where D^+ is pseudoinverse of D. A sparse representation of this equation in l^0 norm sense is $min_x||x||_0$ subjected to $y = Dx$ which is a NP hard problem, however there are solutions, for example Orthogonal Matching Pursuit method grantees the solution in terms of sparse combinations of dictionary elements. Our objective function is

$$min\{\lambda_1 \sum_{1:N}(||y_i - Dx_i||_2)^2 + \lambda_2 \sum_{1:N}||x||_0 + \lambda_3 F(C)\} \quad (1)$$

Here, the λ_i are to regularize the function between three components. The first is the error of regeneration utilizing dictionaries. Correct dictionary of the organ will provide minimum error, with minimum sparsity that is the second part of the equation. And the last part is the Fisher discriminative term to introduce an explicit selectivity by maximizing the ratio of inter to intra-class variance between contour shape characteristics. The contour shape characteristics are obtained by using bending function [16], which provides the sparsest, scale and rotation invariant presentation of contours, and offers the set of maximal bending points. The focus of the first part of Eq.1 is on entire image registration to a template image, and the last part is on component-wise. Testing a contour C_i against other mean contour vectors, such that the one that a k^{th} contour C_k is assigned to, $min_{m=1:M}\{(C_k - \bar{C}_m)(C_k - \bar{C}_m)^T\}$ where M is the number of organs at each CT slice, and $\bar{C}_m$ is the mean vector of the m_{th} organel contour dictionary. Then the $F(C)$ discriminant selectivity criteria in equation 1, is defined as

$$FC = \frac{||\sum_{i=1:M,j:M,j\neq i}(C_i - \bar{C}_j)(C_i - \bar{C}_j)^T||_2^2}{||\sum_{i=1:M,}(C_i - \bar{C}_i)(C_i - \bar{C}_i)^T||_2^2} \quad (2)$$

Eqns.2, and 1, give an optimal set of assignment for organs, after each contour is assigned to an organ in l^2 norm sense.

Fig. 5. (Left) Over and (Right) Under segmented regions of abdominal CT Scout image 17 with different thresholdings where we were able to obtain correct contours only partially.

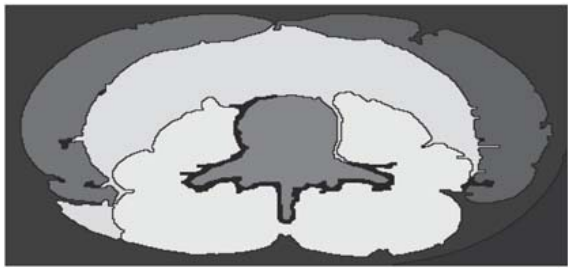

Fig. 6. Segmented abdominal region of CT Scout image slice 17 from the curvelet subbands after morpho-processing. Psoas, Erector Spinae Muscle, Quadratus Lumborum Muscle, Internal Oblique and External Obligue, Tranversus Abdominus, Rectus Abdominus Muscle

V. Experimental results

We used 35 axial non-contrast scout images taken with $3mm$ distances from Lumbar $L4/L5$ region of anonymized five normal adults. Only 15 of these images are used to train silhouettes library, and the remaining are used for testing. The organs explicitly visible, abdominal muscles stretching at the left and right lateral quadrants, and vertebrate, and muscles at the medial posterior proximity of the vertebrate are detected as presented in Fig.6, to employ principle of exclusion by assuming that the residual area is the abstract representation of mesentery. We determine final contours by using dictionaries that are trained from the corresponding subbands of the organs. We took the anatomical positioning into account and using rotation and scale invariant bend functions which yield a non-iterative image registration based on the trained contours.

VI. Conclusion

In this paper, we presented an embedded scheme to detect abdominal organs from DICOM images in three stages, curvelets, morphological edge enhancement and a registration stage wrt template dictionaries of abdominal organs. Our approach is novel in the sense of using the gestalts of these organs with lower entropy, we approximately extract the mesenteric region which has a nature of higher uncertainty. In 6 CT images out of 10, the boundaries of mesentery was completely extracted. To achieve the same results with the wavelets was not possible.Our preliminary results of the success ratio with curvelets at this stage is satisfactory, just above 60% of correct segmentation, registration and identification. The research is continuing to take into account texture information and other anatomical dependencies and will be further extended to 3D volume images.

Fig. 7. Approximate mesenteric area completely extracted, CT slice 17.

ACKNOWLEDGMENT

M Sakalli gives his special thanks to radiologists Dr. Murat Ulusoy, MD, Dept of Radiology, Gelişim Univ, and to Dr. Gökhan Uçar, MD, American Hosp. Dept of Radiology, for the data provided and their evaluations of CT images. M Sakalli also thanks to Senior Lecturer Dr Nakkeeran. Kaliyaperumal, Univ. of Aberdeen.

References

[1] E.A. Barclay, Models of the Human Stomach Showing its Form Under Various Conditions, J. Anatomy, v 54, no 2-3, pp 258-269, Jan, 1920.
[2] R. O'Rahilly, F. Müller, Basic Human Anatomy, A Regional Study of Human Structure, Saunders, 1983.
[3] PM. Hanno, Painful Bladder Syndrome Interstitial Cystitis and Related Disorders, p.330-70. Diagnosis by Exclusion. Ch10., Campbell-Walsh Urology. 9th ed. Saunders, 2007
[4] S. Kim, KJ. Yun and IS. Kweon, Object Recognition Using a Generalized Robust Invariant Feature and Gestalt's Law of Proximity and Similarity, CVPRW'06, 2006
[5] A.L. Zobrist, W.B. Thompson, Building a Distance Function for Gestalt Grouping, IEEE Trans on Comp, v24 n7, pp718-28, July, 1975
[6] J. Ma, G. Plonka, The Curvelet Transform: A review of recent applications, IEEE Signal Proc. Mag., v27, no2, pp.118-33, March, 2010
[7] G. Peyre, S. Mallat, Surface compression with geometric bandelets, ACM Trans. on Graphics (Proc. SIGGRAPH 05), v 24, pp 601-8, 2005
[8] T. Aydin, Y. Yemez, E. Anarim, B. Sankur, Multidirectional and Multiscale Edge-detection Via M-Band Wavelet Transform, IEEE IP, v 5, no 9, pp 1370-77, Sept 1996,
[9] E. J. Candès, D. L. Donoho, Ridgelets: a key to higher-dimensional intermittency?, Philosophical Trans of the Royal Society A, v 357, no 1760, pp 2495-509, 1999
[10] E. J. Candès, L. Demanet, D. L. Donoho, L.Ying, Fast Discrete Curvelet Transforms, Techn. Report, 2005
[11] E. J. Candès, L. Demanet, D. L. Donoho, L. Ying, Fast Discrete Curvelet Transforms, Multiscale Modeling and Simulation, v 5, no 3, pp 861-99, 2006
[12] T. Gebäck, P. Koumoutsakos, Edge detection in microscopy images using curvelets, BMC Bioinformatics, v 10, no 75, 2009
[13] R. Rubinstein, M. A Bruckstein, M. Elad, Dictionaries for Sparse Representation Modeling, Proc. IEEE, v 98, p.1045-57, June 2010
[14] B. Olshausen, D. Field, Emergence of Simple-Cell Receptive Field Properties by Learning a Sparse Code for Natural Images, Nature, no 381, 607-9, 1996
[15] J. Daugman, Complete Discrete 2-D Gabor Transforms by Neural Networks for Image Analy and Compres v36, no7, pp 1169-79, 1988
[16] A.M.N. Fu, H. Yan, K. Huang, A Curve Bend Function based Method to Characterize Contour Shapes, Pattern Recognition, v 30, no 10, pp 1661-71, 1997.
[17] M. Sakalli, KM. Lam, H. Yan, A Faster Converging Snake Algorithm to Locate Object Boundaries, IEEE Trans IP, no 5, pp 1182-91, 2006
[18] DJ. Barbosa, J. Romus, JH. Correia, CS. Lima, Automatic Detection of Small Bowel Tumors in Capsule Endoscopy based on Color Curvelet Covariance Statistical Texture Descriptors, Conf Proc IEEE Eng Med Biol S. pp 6683-6, 2009.